

# A Lithography-Free and Field-Programmable Photonic Metacanvas

Kaichen Dong, Sukjoon Hong, Yang Deng, He Ma, Jiachen Li, Xi Wang, Junyeob Yeo, Letian Wang, Shuai Lou, Kyle B. Tom, Kai Liu, Zheng You, Yang Wei, Costas P. Grigoropoulos, Jie Yao,\* and Junqiao Wu\*

The unique correspondence between mathematical operators and photonic elements in wave optics enables quantitative analysis of light manipulation with individual optical devices. Phase-transition materials are able to provide real-time reconfigurability of these devices, which would create new optical functionalities via (re)compilation of photonic operators, as those achieved in other fields such as field-programmable gate arrays (FPGA). Here, by exploiting the hysteretic phase transition of vanadium dioxide, an all-solid, rewritable metacanvas on which nearly arbitrary photonic devices can be rapidly and repeatedly written and erased is presented. The writing is performed with a low-power laser and the entire process stays below 90 °C. Using the metacanvas, dynamic manipulation of optical waves is demonstrated for light propagation, polarization, and reconstruction. The metacanvas supports physical (re)compilation of photonic operators akin to that of FPGA, opening up possibilities where photonic elements can be field programmed to deliver complex, system-level functionalities.

Mathematical operators are generally used in wave optics to quantify the light manipulation of photonic devices, and different photonic devices correspond to specifically fixed mathematical operators,<sup>[1]</sup> which indeed leads to principal and experimental limitations. On the one hand, *in situ* modification of the corresponding mathematical operators is necessary

to fulfill the functionality of an optical reconfigurable system; on the other hand, probing into the time-resolved observation of photonic phenomena requires real-time evolution of those mathematical operators. As such, rewratability, with successful examples in other fields like field-programmable gate arrays (FPGA),<sup>[2]</sup> would create new optical functionalities via (re) compilation of photonic operators,<sup>[3]</sup> and thus inevitably attracts vast attention in the field of photonics. Previous attempts at realizing the reconfigurability used micro/nanomechanical metamaterials,<sup>[4–6]</sup> liquid crystals<sup>[7]</sup> or amorphous-crystalline phase-transition materials,<sup>[8]</sup> which are limited in terms of functionality, pixel density, efficiency, fabrication/reconfiguration cost or high working temperature (>623 °C).<sup>[9]</sup> It is much desired to utilize

phase-transition materials to reconfigure photonic elements in a fast, scalable, cost-effective, and lithography-free way at or near room temperature.

In this work, we present an all-solid, rewritable metacanvas for photonic applications, on which arbitrary photonic devices can be rapidly and repeatedly written and erased for real-time

Dr. K. Dong, Y. Deng, Dr. X. Wang, S. Lou, K. B. Tom, Prof. J. Yao, Prof. J. Wu  
Department of Materials Science and Engineering

University of California  
Berkeley, CA 94720, USA  
E-mail: yaojie@berkeley.edu; wuj@berkeley.edu

Dr. K. Dong, K. B. Tom, Prof. J. Yao, Prof. J. Wu  
Materials Sciences Division  
Lawrence Berkeley National Laboratory  
Berkeley, CA 94720, USA

Dr. K. Dong, Prof. Z. You  
State Key Laboratory of Precision Measurement Technology  
and Instruments  
Department of Precision Instrument  
Tsinghua University  
Beijing 100084, P. R. China

Prof. S. Hong, Prof. J. Yeo, L. Wang, Prof. C. P. Grigoropoulos  
Department of Mechanical Engineering  
University of California  
Berkeley, CA 94720, USA

 The ORCID identification number(s) for the author(s) of this article  
can be found under <https://doi.org/10.1002/adma.201703878>.

DOI: 10.1002/adma.201703878

Prof. S. Hong  
Department of Mechanical Engineering  
Hanyang University  
55 Hanyangdaehak-ro, Sangnok-gu, Ansan, Gyeonggi-do  
15588, Republic of Korea

Prof. H. Ma, J. Li, Prof. Y. Wei  
Department of Physics and Tsinghua-Foxconn  
Nanotechnology Research Center  
Tsinghua University  
Beijing 100084, P. R. China

Prof. J. Yeo  
Department of Physics  
Kyungpook National University  
80 Daehak-ro, Bukgu, Daegu 41566, Republic of Korea

Prof. K. Liu  
State Key Laboratory of New Ceramics and Fine Processing  
School of Materials Science and Engineering  
Tsinghua University  
Beijing 100084, P. R. China

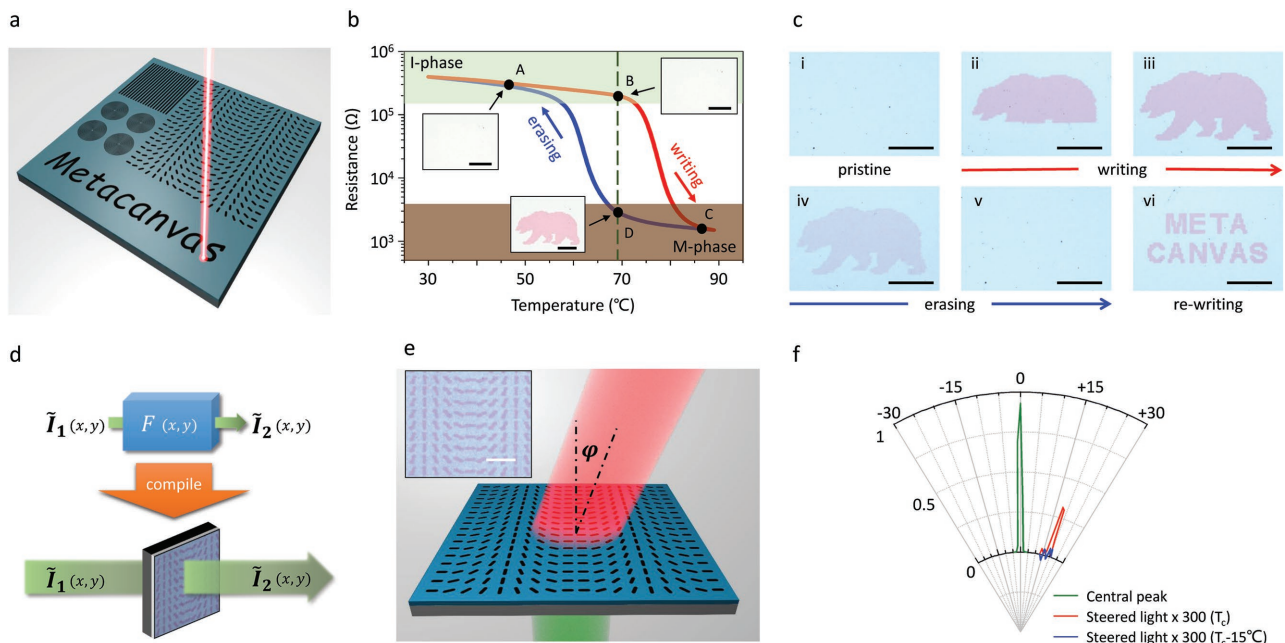


**Figure 1.** A rewritable metacanvas. a) Schematic of laser writing different photonic operator patterns on a metacanvas. b) Temperature-dependent resistance of a VO<sub>2</sub> film, where the transition temperature ( $T_c$ ) is denoted by a vertical dashed line. Insets A and B: Unpatterned VO<sub>2</sub> film (all in I-phase). Inset D: The VO<sub>2</sub> film (global temperature kept at  $T_c$ ) is laser written with a pattern of a bear in the M-phase. c) Optical images from writing and erasing process on the metacanvas: i-iii) a pattern of a bear (M-phase) is written onto an I-phase VO<sub>2</sub> film, iv,v) then erased by decreasing the global temperature, vi) and another pattern of the word "METACANVAS" is written subsequently. d) Diagram showing the mathematical matrix ( $F$ ) is compiled onto a metacanvas in the form of a photonic operator for manipulation of light waveform ( $\tilde{I}$ ). e) Schematic of a metacanvas programmed as a beam steerer with a steering angle  $\varphi$ . Inset: Optical image of the beam steering phase array compiled on the metacanvas. f) Normalized, measured light intensity as a function of the propagation direction angle  $\varphi$ . Scale bar is 100  $\mu\text{m}$  in (b) and (c), and 10  $\mu\text{m}$  in (e).

manipulation of light waves. Different patterns can be written and erased on the same metacanvas successively. The writing is performed with a low-power laser and the entire process stays below 90 °C. Dynamic manipulation of optical waves is demonstrated with the metacanvas, specifically light propagation, polarization, and reconstruction. The metacanvas supports physical (re)compilation of photonic operators akin to that of FPGA, thus realizing the in situ modification of the corresponding mathematical operators of the metacanvas. This dynamic optical system without moving parts opens possibilities where photonic elements can be field programmed to deliver complex, system-level functionalities.

The metacanvas is realized using the hysteretic metal-insulator phase transition (MIT) of polycrystalline vanadium dioxide (VO<sub>2</sub>) films. Figure 1a shows the schematic of a metacanvas being micropatterned with a focused laser beam. VO<sub>2</sub> undergoes a temperature-driven, reversible transition from the insulating (I) to the metallic (M) phase when heated above its transition temperature ( $T_c = 68$  °C).<sup>[10]</sup> These two phases differ drastically in their physical properties: the electron density ( $1.9 \times 10^{23} \text{ cm}^{-3}$  for the M-phase vs  $1.9 \times 10^{19} \text{ cm}^{-3}$  for the I-phase), relative dielectric constant ( $-35 + 119i$  vs 4.9 near the operation wavelength of 10.6  $\mu\text{m}$  in this work), and color (dark green vs bright yellow under white light illumination) are all distinct,<sup>[10,11]</sup> thus attracting much attention in various fields.<sup>[12-14]</sup> These contrasts, together with the MIT hysteresis of polycrystalline VO<sub>2</sub> films, lay the material foundation that enables the all-solid metacanvas for nonvolatile patterning and erasing.

As illustrated in Figure 1b, we first globally heat the VO<sub>2</sub> film from room temperature (cooler than Point A) to  $T_c$  (Point B), and the entire film is still in the I-phase. Subsequently, a laser is focused onto the film to locally heat the VO<sub>2</sub> to the M-phase (Point C). When the laser is turned off or moves to other regions, the laser-heated region will still stay in the M-phase (Point D) owing to the hysteresis.<sup>[15]</sup> Hence, a nonvolatile M-phase pattern is written onto the I-phase film. The pattern can easily be erased by reducing the global temperature of the entire film beyond the hysteresis (e.g., to Point A). Upon reheating to Point B, the film is reset and ready for rewriting a new pattern in the same region. This process is illustrated in Figure 1c, as well as shown in Video S1 (Supporting Information). As such, nearly arbitrary patterns of the M-phase can be written, erased, and rewritten onto the I-phase film, hence forming a canvas to "field program" various metaphotonic elements.

Such a rewritable metacanvas is ideal to physically realize mathematical operators for the manipulation of light. This process is similar in spirit to compilation in electrical engineering: to realize a desired logic in the form of a software program, it is compiled into FPGA using an assembly language. In such a process, the speed of compilation and the programmability of FPGA are critically important. In analogy, to realize the desired mathematical operator to manipulate light, it is rapidly<sup>[16]</sup> compiled onto the metacanvas using the "photonic assembly language" (Figure 1d), which can be optical gratings,<sup>[17,18]</sup> metasurfaces,<sup>[8,19-22]</sup> holography,<sup>[23,24]</sup> metatronics,<sup>[25]</sup> etc.

Therefore, the metacanvas is analogous to the FPGA in three aspects: the compilation of mathematical logics into hardware to suit different applications; the resultant multifunctionalities within one single device; and the real-time reprogrammability after the device is already deployed. Unlike previous lithographically made  $\text{VO}_2$  devices that can only be switched ON/OFF with permanent patterns and fixed functionalities,<sup>[26–36]</sup> the lithography-free metacanvas is fully reconfigurable in terms of both patterns and functionalities (see Section S2 in the Supporting Information for detailed comparison). As such, the rapid, cost-effective, and reversible compilation of photonic operators on the rewritable metacanvas with lithography-free, micrometer-sized features potentially enables a rich collection of photonics research and applications. Note that the thickness of the  $\text{VO}_2$  film used is only 200 nm and the probe beam wavelength is 10.6  $\mu\text{m}$ , forming a wavelength-thickness ratio as high as 53 for all the photonic operators compiled. The writing beam used in the following experiments is a 532 nm continuous laser with a power around 1 mW and a diameter  $<1\text{ }\mu\text{m}$ , such that a feature size of  $\approx 1\text{ }\mu\text{m}$  is achieved. Here, we start by dynamically compiling a beam steering operator<sup>[20,37,38]</sup> on the metacanvas as a proof of concept, based on which we show a more general prototype for a reconfigurable photonic system. Finally, we develop the concept of and demonstrate a physical simulator utilizing the fast (re)compilation of operators on the metacanvas.

Electromagnetic phase arrays have found various applications ranging from radar, communication,<sup>[37]</sup> biomedical sciences,<sup>[39]</sup> holography,<sup>[23,24]</sup> to optical tweezers.<sup>[40]</sup> Currently, large-scale integrated phase array has been reported,<sup>[38]</sup> but a cost-effective way to implement large-scale, lithography-free, and rapidly reconfigurable phase arrays is much desired to boost these applications. Here, we first test a basic function of the phase array, beam steering. Figure 1e shows the diagram of the beam steering process with the metacanvas. The designed phase array is compiled onto the metacanvas, which steers the input light beam to an angle of  $\varphi_i$  as well as changes the handedness of the steered beam.<sup>[24]</sup> In the experiment, a steered beam was indeed observed along the designed direction (Figure 1f). As we erased the phase array on the metacanvas by decreasing the global temperature, the steered beam vanished, so a new photonic operator can be compiled afterward onto the same metacanvas for beam steering in different directions, thus verifying the (re)compilation of operators on the metacanvas.

As a versatile platform capable of “free-style” (re)compilation of operators, the metacanvas can go beyond device-level applications such as the beam steerer and enable construction of a comprehensively reconfigurable photonic system. Here, we demonstrate a prototype of such reconfigurable system using two metacanvases for time-resolved observation of dynamic transitions. Transitions between physical phenomena have been heavily investigated in attempt to reveal the otherwise hidden dynamics in various contexts, such as quantum systems<sup>[41]</sup> and topological phase transition.<sup>[42]</sup> However, in photonic systems, it is rather difficult or even impossible to experimentally achieve smooth transitions without interrupting the optics. Aided with *in situ* programming capabilities, a metacanvas-based system enables real-time reconfiguration of

photonic operators to manipulate light, thus opening up new opportunities for resolving and probing dynamic transitions. Again as a proof of concept, we use manipulation of structured light with structured devices<sup>[43]</sup> as an example. Concentric-ring gratings have been studied intensively for exploration of cylindrical vector and orbital angular momentum with possible applications such as tight focusing and structuring of light.<sup>[43]</sup> A circularly polarized beam transmitting through the grating generates a doughnut-shaped light field with a dark center due to high transmittance of the radial component of the light beam, while a linearly polarized incident beam results in a two-lobe-shaped light field.<sup>[43]</sup>

The diagram of achieving such transition is shown schematically in Figure 2a. Sequentially erasing operators  $F_1$  and  $F_2$  would enable the transition from  $\tilde{I}_3$  to  $\tilde{I}_3$ , and finally  $\tilde{I}_1$ . The definition of the operator  $F_i$ , light waveform  $\tilde{I}_i$ , and detailed formulas are summarized in Section S4 in the Supporting Information. The experimental setup is shown in Figure 2b, where two metacanvases are used. The first metacanvas programmed as a linear polarizer ( $F_1$ ) transforms the circularly polarized light ( $\tilde{I}_1$ ) into linear polarized light ( $\tilde{I}_2$ ), which is further transformed into a two-lobe pattern ( $\tilde{I}_3$ ) by a concentric-ring grating ( $F_2$ ) compiled on the second metacanvas. Prior to the transition experiment, we separately characterized the performance of the linear polarizer at variable temperatures, which proved that  $F_1$  was correctly compiled, functioning, and erasable (Figure 2c). The polarization ratio of this linear polarizer is maximized and equal to 4.5 at  $T_c$  and gradually decreases to about 1 at  $T_c - 15\text{ }^\circ\text{C}$  when the pattern is nearly completely erased. The polarization ratio depends on temperature in a way that is in full agreement with the cooling-down curve of conductance derived from Figure 1b (see Section S7 in the Supporting Information), proving that the erasing of  $F_1$  indeed arises from the MIT of  $\text{VO}_2$ .<sup>[26]</sup> The concentric-ring grating was also similarly characterized and its performance was confirmed. As we assembled them as an optical system in Figure 2b, a two-lobe pattern ( $\tilde{I}_3$ ) was detected, as shown in Figure 2di. When  $F_1$  was being erased, we observed a smooth transition from the two-lobe pattern  $\tilde{I}_3$  to a doughnut pattern  $\tilde{I}_3$ , thanks to the smooth transition of the light before  $F_2$  from linear polarization to circular polarization. The reduced optical contrast of the patterns, which are practically new operators, carries the information of intermediate states. Finally, when  $F_2$  was also completely erased, the doughnut pattern vanished and the output returned the light field of  $\tilde{I}_1$  since there is no operator acting on it (Figure 2dvii). This process is shown in Video S2 (Supporting Information). We note that what is plotted in Figure 2d is the transmission ratio in order to explicitly show the pattern (see the Experimental Section). Thus, the metacanvas based optics could enable dynamical transition in optics without physically replacing the optical components. New photonic operators can be subsequently compiled onto these metacanvases, hence realizing system-level reconfiguration, potentially a valuable merit for applications such as optical computing.<sup>[44]</sup>

To further employ such photonic operator recompilation as demonstrated by the reconfigurable photonic system, we use the metacanvas to experimentally simulate the design of optical elements, thereafter termed as a physical simulator. Physical

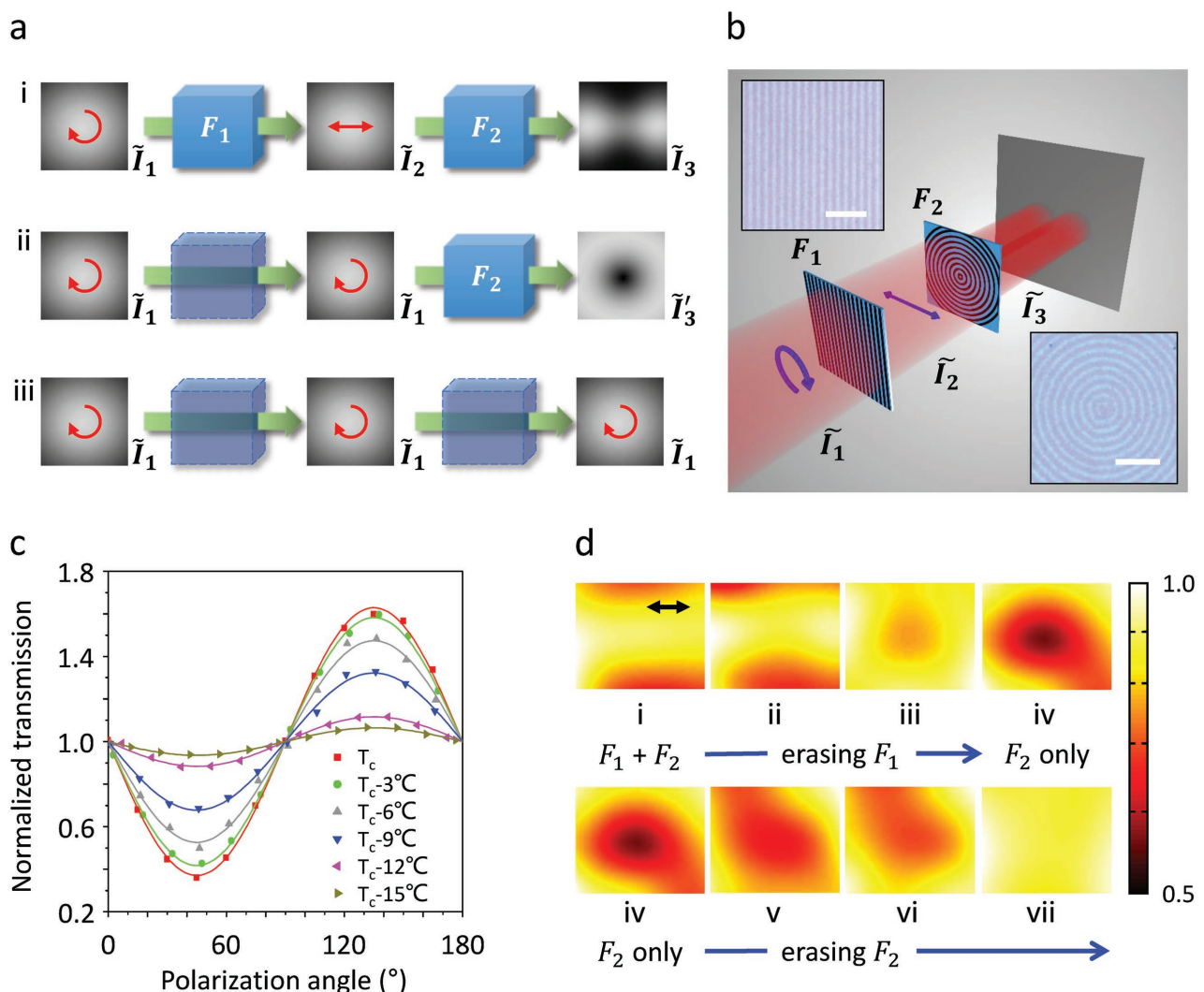


**Figure 2.** Dynamic compilation of operators on the metacanvas. a) Schematic diagram of light manipulation with dynamic control of operators. b) Schematic of the experimental setup. Inset: Optical images of a linear polarizer  $F_1$  (top left) or a concentric-ring grating  $F_2$  (bottom right) compiled on the metacanvas. Scale bar: 10  $\mu\text{m}$ . c) Evolution of the normalized, polarization-dependent light transmission from the linear polarizer as temperature is decreased from  $T_c$  to  $T_c - 15^\circ\text{C}$ . d) Transmitted light intensity normalized by the profile of the incident light intensity. i) Two-lobe pattern where the arrow shows the polarization direction. ii-iv) Transition from the two-lobe pattern ( $F_1 + F_2$ ) to a doughnut pattern ( $F_2$  only) when the linear polarizer ( $F_1$ ) is erased. iv-vii) Fading of the doughnut pattern when the concentric-ring grating ( $F_2$ ) is also erased.

simulation is generally used in engineering projects to evaluate and compensate random errors arising from real-world applications that cannot be precaptured by theoretical calculation or computer simulation<sup>[45]</sup> but are critical in fields such as holography. One deep-rooted problem in holography is the mismatch between the designed and experimental results caused by ubiquitous experimental errors, such as fabrication error, detector resolution, laser noise, and diffraction distortion.<sup>[46]</sup> Although numerical full-wave simulation is able to partially solve these problems, the solution is severely limited by the memory size and computation power of the simulating computer. As a result, it has not been possible to simulate large-scale holograms with billions of meshes, let alone the random influence of optical setups involved.<sup>[47]</sup> The metacanvas, with the advantages of lithography free, economical, and rapid recompilation,

presents an approach to simulate the hologram with a physically real system, i.e., a physical simulator.

The work flow of physical simulation is depicted in Figure 3a, where the analytically designed hologram  $F_d$  is compiled onto a metacanvas to output an experimental holographic image. The difference between the designed ( $\tilde{I}_d$ ) and the physically simulated ( $\tilde{I}_p$ ) images is analyzed to find the lumped experimental error ( $F_e$ ). In the next step, a correction ( $F_e^{-1}$ ) is added to the design to compensate  $F_e$ , hence achieving the error-corrected output ( $\tilde{I}_i$ ). Such corrected design ( $F_d$ ) can then be applied to real-world fabrication of holograms. To demonstrate a proof of concept of this process, we compiled onto the metacanvas a computer-generated hologram of an image consisting of two spots, each with the size of a pixel (Figure 3b). The design (i, ii) and the experimental observation (iii) are shown in Figure 3c.

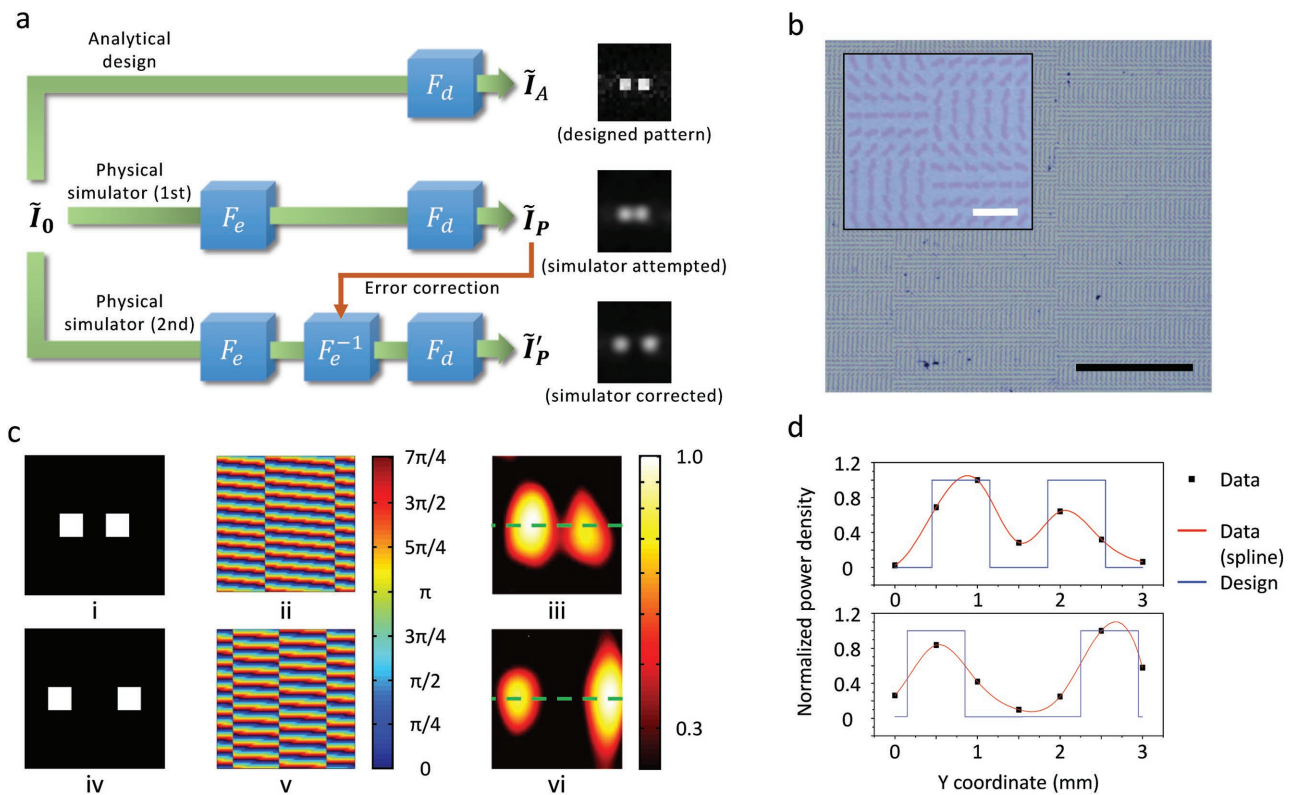


**Figure 3.** The metacanvas functioning as a holographic physical simulator. a) Diagram showing the image correction process using the physical simulator with schematic images. The first attempt in the physical simulator output ( $\tilde{I}_P$ ) includes the lumped experimental error ( $F_e$ ) and the designed phase distribution ( $F_d$ ). This error information can then be identified and taken into consideration in the second-round design ( $F_d = F_e^{-1} F_d$ ) in the physical simulation to eliminate the error. The corrected phase array ( $F_d$ ) can then be used in real implementation to yield an ideal image as designed. b) Optical images of a hologram compiled on the metacanvas with different magnifications. Note that this hologram consists of the information for the two-spot image and  $18^\circ$  beam steering phase distribution, and thus is different from that in Figure 1e. Scale bar: 100  $\mu\text{m}$  (main) and 10  $\mu\text{m}$  (inset). c) Target two-spot images, the corresponding calculated phase distribution, and the experimental holographic images with i–iii) one-pixel and iv–vi) two-pixel separation. Note that (i) and (iv) only show the middle parts of the full images, and (ii) and (v) have taken the beam steering phase into consideration. d) Comparison between the analytical design and the physical simulator output data along the horizontal dashed lines in the holographic images in (ciii,vi).

The experimental result (iii) in Figure 3c shows that the two spots were not separated sufficiently far from each other, resulting in an overlap between the two spots. We then fixed the error by adding one more pixel between the spots (iv, v), which led to a complete separation of the two spots (vi). The comparison between the design and the experimental data clearly shows the limitation of the analytical designing (Figure 3d). Therefore, by comparing the experimental results to the analytical design, the metacanvas-based physical simulator effectively processes a full-wave simulation breaking the computational limitations, providing a fast, cost-effective, lithography-free approach to optimize metaholotonic elements before their real-world fabrication.

In conclusion, we have exploited the  $\text{VO}_2$  phase transition to attain real-time reconfigurability and field programmability of photonic devices, and achieved rapid (re)compilation of various photonic operators on the metacanvas for full light manipulation in both space and time dimensions. From the high-speed, large-scale, “free-style” writing and erasing, the dynamic compilation of photonic operators has the potential to enable unprecedented applications (e.g., real-time analysis and control

of photonic devices) as well as basic research (e.g., probing into time-dependent optical processes). We note that all the experiments (including Videos S1 and S2 in the Supporting Information) we show in this work were completed with only three  $\text{VO}_2$  films, which have undergone several tens of damage-free writing–erasing processes under ambient condition, exhibiting great versatility and stability. Different patterns have been repetitively written and erased on the same film, thus proving the context of rewritability.

The technical specifications of the metacanvas are analyzed as follows: First, the patterns shown in Figures 1e, 2b, and 3b were written at a speed of  $0.03\text{--}2 \text{ mm s}^{-1}$ , depending on the complexity of the patterns. The current writing speed is only limited by the stability of the direct laser writing system, in which high writing speeds result in strong mechanical vibration. Considering the feature size and the laser power (see the Experimental Section), the energy cost to pattern the metacanvas is calculated to be  $\approx 600 \text{ nJ } \mu\text{m}^{-2}$ , which is higher than the theoretical lower bound of the writing power of  $0.064 \text{ nJ } \mu\text{m}^{-2}$  because of nonideal optical absorption of the  $\text{VO}_2$  films as well as heat dissipation. Second, the theoretical lower bound of standby

power of the metacanvas is the heat loss from the sample surface to air, as the other heat losses (to solid heat sinks) can be minimized by design for good heat isolation. This is estimated to be  $\approx 700 \mu\text{W}$  per sample size of  $1.28 \times 1.28 \text{ mm}^2$ . Practically, microheaters with a similar geometry can maintain  $\approx 68^\circ\text{C}$  with a power consumption on the order of  $\approx 10 \text{ mW}$ .<sup>[48,49]</sup> Third, the relaxation time of the metacanvas is limited by the cooling rate rather than the intrinsic phase transition speed of  $\text{VO}_2$ .<sup>[16]</sup> In the experiment, it was observed that the patterns can be erased in  $\approx 1 \text{ s}$  at room temperature. In the extreme case that air cooling is the only heat loss, numerical calculation shows that it takes  $\approx 27 \text{ s}$  to cool down an Si chip ( $1 \times 1 \times 0.5 \text{ mm}^3$ , imitating the metacanvas) from  $68$  to  $45^\circ\text{C}$  to erase all M-phase patterns (see Section S9 in the Supporting Information for details).

The performance of the photonic operators compiled on the metacanvas can be further improved by optimizing the feature size and shape, the film thickness, and the material quality. Current limitations for unleashing the full potential of the metacanvas are related to our facilities rather than the metacanvas itself. Further improvements in the metacanvas can be made at least in two aspects: first, switching the laser writing to electrical control of metacanvas will potentially yield a friendlier device footprint for some integrated electronic systems; second, the technology of metacanvas can be applied to other materials with first-order phase transition and a hysteresis akin to that of  $\text{VO}_2$  films,<sup>[50]</sup> potentially expanding the spectral range and working condition. In all, aided with more advanced facilities, one can envision to further apply the metacanvas technology for more advanced applications, such as optical computing<sup>[44]</sup> or fully reconfigurable photonic circuitry.<sup>[51]</sup> It is also possible to build dynamic optical systems without moving parts, where a wide range of functionalities can be customized in situ by repeatedly programming and coding the metacanvases.

## Experimental Section

**$\text{VO}_2$  Growth and Characterization:**  $\text{VO}_2$  films were deposited onto double-side polished, undoped Si substrates in a DC magnetron sputtering system using a high-purity vanadium metal target. The sputtering was carried out with a flowing gas mixture (49.7 sccm Ar and 0.3 sccm  $\text{O}_2$  under 0.55 Pa for 30 min, DC power of 60 W) at room temperature. After the  $\text{VO}_2$  deposition, it was annealed in a low-pressure  $\text{O}_2$  atmosphere ( $3 \times 10^{-2} \text{ mbar}$ ) at  $450^\circ\text{C}$  for 10 min to facilitate the crystallization. The resistance hysteresis curve of the  $\text{VO}_2$  shown in Figure 1b was measured using a probe station and a home-made heating stage with a Lakeshore 325 temperature controller.

**Laser Writing:** The temperature control (heating and cooling) was achieved using Lakeshore 325 (and/or 321) temperature controller(s) and home-made heating stages which consisted of Pt temperature sensors and Kapton insulated flexible heaters.

For the characterization experiments, an LRS-0532 diode pumped solid-state continuous-wave laser (Laserglow Technologies) was used for the laser writing at 532 nm wavelength. Besides the laser, key components in the direct laser writing system included an Olympus 100  $\times$  lens (NA = 0.95, infinity corrected), a nanopositioning stage (Aerotech, ANT130-XY series), and a mechanical shutter (Thorlabs). The laser power irradiated at the  $\text{VO}_2$  film was 1.14–1.25 mW, with a diameter less than 1  $\mu\text{m}$ . The writing speeds for the polarizers, concentric rings, and the metasurface were  $2 \text{ mm s}^{-1}$ ,  $0.05\text{--}0.2 \text{ mm s}^{-1}$ , and  $0.03 \text{ mm s}^{-1}$ , respectively. As such, the intrinsic spatial resolution is set by the thermal diffusion length in  $\text{VO}_2$  and is estimated to be

$\approx 100 \text{ nm}$  within the laser exposure time ( $<40 \text{ ms}$ ) of the area of  $1 \mu\text{m}^2$ , which is on the similar order of the grain size of the  $\text{VO}_2$  film (Figure S2, Supporting Information). Also, the latent heat of  $\text{VO}_2$  phase transition helps prevent the leakage. Hence, it can be concluded that finer features can be achieved with advanced writing tools.

For writing the patterns of the bear and the word "METACANVAS", a  $20 \times$  lens (Mitutoyo) was used instead, and the laser power irradiated at the  $\text{VO}_2$  film was 11.5 mW, which had a diameter of approximately 3  $\mu\text{m}$ . The movement of the nanopositioning stage and the ON/OFF of the mechanical shutter were computer programmed and automatically controlled, as shown in Video S1 (Supporting Information), where a CCD camera was used for *in situ* observation and recording.

**Metacanvas Characterization:** A  $\text{CO}_2$  laser (DIAMOND C-20A, Coherent Inc.), with a waveform generator (33600A series, Keysight Technologies Inc.), was used for generating the  $10.6 \mu\text{m}$  laser radiation in all the characterization experiments. A commercial wire grid linear polarizer (WP25M-IRC, Thorlabs) and a  $90^\circ$  phase retarder (Ophir) were used for the creation of the circularly polarized light. The subsequent integrated power measurement in Figure 2c was carried out using a high-sensitivity thermal power sensor (S401C, Thorlabs), where each data point is the average of 20 measurements continuously recorded at 10 Hz. The mapping of intensity distribution was achieved with pixel-by-pixel scanning: an iris and the power sensor (S401C) were integrated onto a three-axis nanomax stage (Thorlabs) controlled by a three-channel APT benchtop stepper motor controller (BSC203, Thorlabs). Similarly, each data point in the mapping is averaged from 10 consecutive measurements. B-spline interpolation was applied to all the mapping data using Mathematica.

In the beam steering experiment, the circularly polarized light transmitted through the metacanvas programmed as a phase array. A focusing lens was positioned behind the metacanvas. Since the distance between the metacanvas and the lens was equal to its focal length, the steered light was focused at the focal plane on the other side, where a 2D mapping was conducted. After converting the position information at the mapping plane into the steered angle, we obtained data to plot Figure 1f.

For characterization of the metacanvas programmed as a linear polarizer, the generated circularly polarized light went through the metacanvas, another commercial linear polarizer (WP25M-IRC, Thorlabs), and then finally into the power sensor (S401C) for integrated power measurements. The transmittance power was measured as a function of the rotation angle of the commercial linear polarizer. We fitted to the data points with sine functions ( $f_i = A_i \sin(\omega_i \vartheta + \delta_i) + B_i$ ) and then normalized them with the value of  $B_i$  to plot Figure 2c. In a separate characterization experiment, the metacanvas was programmed as a concentric-ring grating. The commercial linear polarizer (WP25M-IRC) was positioned before the metacanvas to image the two-lobe pattern, while the doughnut pattern was mapped without the commercial linear polarizer, i.e., the circularly polarized light went directly through the metacanvas. We divided the experimentally recorded 2D light intensity map with the input Gaussian beam intensity profile to obtain the 2D transmission ratio map, as shown in Figure S9 in the Supporting Information. Figure 2d was obtained with the same setup as shown in Figure 2b and the same image processing method described above. We thus resolved the transition process (see Video S2 in the Supporting Information) from Figure 2d using interpolation.

Fast Fourier transform was used to generate a hologram, which is shown in Figure 3a,c. To separate the holographic image from the transmitted main peak without degrading the signal-to-noise ratio, we added an extra  $18^\circ$  beam steering phase information to the hologram. The experimental realization of the holography utilized the same setup as the beam steering experiment.

## Supporting Information

Supporting Information is available from the Wiley Online Library or from the author.

## Acknowledgements

K.D., S.H., and Y.D. contributed equally to this work. This work was supported by U.S. NSF Grant No. 1608899. The VO<sub>2</sub> thin films were grown in the Tsinghua-Foxconn Nanotechnology Research Center at Tsinghua University. Some of the fabrication used facilities in the Electronic Materials Group funded by the Director, Office of Science, Office of Basic Energy Sciences, Material Sciences and Engineering Division of the U.S. Department of Energy under contract number DE-AC02-05CH11231. K.D. acknowledges the China Scholarship Council (CSC, Grant No. 201406210211) for financial support. K.D., Y.D., and J. Yao were also supported by the Bakar fellows program of the University of California, Berkeley. H.M. and Y.W. acknowledge the National Natural Science Foundation of China (Grant No. 51472142). The authors are grateful to Prof. K. Jiang, J. Zhong, Qitong Li, Prof. Z. Hou, Y. Rho, X. Lei, Y. Lv, C. Ko, H. S. Choe, Y. Chen, Quanwei Li, J. Kim, T. Van de Goor, J. Xiao, H. Zhu, Z. Gong, E. Cardona, and S. He for helpful discussions.

## Conflict of Interest

The authors declare no conflict of interest.

## Keywords

hysteretic phase transitions, lithography-free writing, metacanvas, real-time reconfigurability, vanadium dioxide

Received: July 12, 2017

Revised: September 27, 2017

Published online: December 11, 2017

- [1] A. Gerrard, J. M. Burch, *Introduction to Matrix Methods in Optics*, Courier Corporation, North Chelmsford, MA 2012.
- [2] S. Brown, J. Rose, *IEEE Des. Test Comput.* **1996**, 13, 42.
- [3] A. Silva1, F. Monticone, G. Castaldi, V. Galdi, A. Alù, N. Engheta, *Science* **2014**, 343, 160.
- [4] N. I. Zheludev, E. Plum, *Nat. Nanotech.* **2016**, 11, 16.
- [5] J.-Y. Ou, E. Plum, J. Zhang, N. I. Zheludev, *Adv. Mater.* **2016**, 28, 729.
- [6] L. Cong, P. Pitchappa, C. Lee, R. Singh, *Adv. Mater.* **2017**, 29, 1700733.
- [7] N. I. Zheludev, *Science* **2015**, 348, 973.
- [8] Q. Wang, E. T. F. Rogers, B. Gholipour, C. Wang, G. Yuan, J. Teng, N. I. Zheludev, *Nat. Photonics* **2016**, 10, 60.
- [9] Z. Sun, J. Zhou, R. Ahuja, *Phys. Rev. Lett.* **2007**, 98, 055505.
- [10] D. Fu, K. Liu, T. Tao, K. Lo, C. Cheng, B. Liu, R. Zhang, H. A. Bechtel, J. Wu, *J. Appl. Phys.* **2013**, 113, 043707.
- [11] M. M. Qazilbash, M. Brehm, G. O. Andreev, A. Frenzel, P. Ho, B. Chae, B. Kim, S. J. Yun, H. Kim, A. V. Balatsky, O. G. Shpyrko, M. B. Maple, F. Keilmann, D. N. Basov, *Phys. Rev. B* **2009**, 79, 075107.
- [12] S. Kumar, M. D. Pickett, J. P. Strachan, G. Gibson, Y. Nishi, R. S. Williams, *Adv. Mater.* **2013**, 25, 6128.
- [13] B. Hu, Y. Ding, W. Chen, D. Kulkarni, Y. Shen, V. V. Tsukruk, Z. L. Wang, *Adv. Mater.* **2010**, 22, 5134.
- [14] L. Pellegrino, N. Manca, T. Kanki, H. Tanaka, M. Biasotti, E. Bellingeri, A. S. Siri, D. Marré, *Adv. Mater.* **2012**, 24, 2929.
- [15] J. Hou, X. Wang, D. Fu, C. Ko, Y. Chen, Y. Sun, S. Lee, K. X. Wang, K. Dong, Y. Sun, S. Tongay, L. Jiao, J. Yao, K. Liu, J. Wu, *Small* **2016**, 12, 3976.
- [16] A. Cavalleri, C. Tóth, C. W. Siders, J. A. Squier, *Phys. Rev. Lett.* **2001**, 87, 237401.
- [17] K. Aydin, V. E. Ferry, R. M. Briggs, H. A. Atwater, *Nat. Commun.* **2011**, 2, 517.
- [18] J. A. Schuller, E. S. Barnard, W. Cai, Y. C. Jun, J. S. White, M. L. Brongersma, *Nat. Mater.* **2010**, 9, 193.
- [19] X. Ding, F. Monticone, K. Zhang, L. Zhang, D. Gao, S. N. Burokur, A. de Lustrac, Q. Wu, C.-W. Qiu, A. Alù, *Adv. Mater.* **2015**, 27, 1195.
- [20] N. Yu, P. Genevet, M. A. Kats, F. Aieta1, J. Tétienne, F. Capasso, Z. Gaburro, *Science* **2011**, 334, 333.
- [21] H. Zhang, M. Kang, X. Zhang, W. Guo, C. Lv, Y. Li, W. Zhang, J. Han, *Adv. Mater.* **2017**, 29, 1604252.
- [22] L. Zhang, S. Mei, K. Huang, C.-W. Qiu, *Adv. Opt. Mater.* **2016**, 4, 818.
- [23] X. Ni, A. V. Kildishev, V. M. Shalaev, *Nat. Commun.* **2013**, 4, 2807.
- [24] L. Huang, X. Chen, H. Mühlenernd, H. Zhang, S. Chen, B. Bai, Q. Tan, G. Jin, K. Cheah, C. Qiu, J. Li, T. Zentgraf, S. Zhang, *Nat. Commun.* **2013**, 4, 2808.
- [25] Y. Sun, B. Edwards, A. Alù, N. Engheta, *Nat. Mater.* **2012**, 11, 208.
- [26] J. Rensberg, S. Zhang, Y. Zhou, A. S. McLeod, C. Schwarz, M. Goldflam, M. Liu, J. Kerbusch, R. Nawrodt, S. Ramanathan, D. N. Basov, F. Capasso, C. Ronning, M. A. Kats, *Nano Lett.* **2016**, 16, 1050.
- [27] R. M. Briggs, I. M. Pryce, H. A. Atwater, *Opt. Express* **2010**, 18, 11192.
- [28] R. Lopez, L. C. Feldman, R. F. Haglund Jr., *Phys. Rev. Lett.* **2004**, 93, 177403.
- [29] D. W. Ferrara, J. Nag, E. R. MacQuarrie, A. B. Kaye, R. F. Haglund Jr., *Nano Lett.* **2013**, 13, 4169.
- [30] J. Y. Suh, E. U. Donev, D. W. Ferrara, K. A. Tetz, L. C. Feldman, R. F. Haglund Jr., *J. Opt. A: Pure Appl. Opt.* **2008**, 10, 055202.
- [31] C. McGahana, K. Appavoo, R. F. Haglund Jr., *J. Vac. Sci. Technol., B* **2013**, 31, 06FE01.
- [32] S. K. Earl, T. D. James, T. J. Davis, J. C. McCallum, R. E. Marvel, R. F. Haglund Jr., A. Roberts, *Opt. Express* **2013**, 21, 27503.
- [33] M. Seo, J. Kyoung, H. Park, S. Koo, H. Kim, H. Bernien, B. J. Kim, J. H. Choe, Y. H. Ahn, H.-T. Kim, N. Park, Q-H. Park, K. Ahn, D. Kim, *Nano Lett.* **2010**, 10, 2064.
- [34] D. J. Shelton, K. R. Coffey, G. D. Boreman, *Opt. Express* **2010**, 18, 1330.
- [35] D. Y. Lei, K. Appavoo, F. Ligmajer, Y. Sonnenfraud, R. F. Haglund Jr., S. A. Maier, *ACS Photonics* **2015**, 2, 1306.
- [36] O. L. Muskens, L. Bergamini, Y. Wang, J. M. Gaskell, N. Zabala, C. de Groot, D. W. Sheel, J. Aizpurua, *Light Sci. Appl.* **2016**, 5, e16173.
- [37] R. C. Hansen, *Phased Array Antennas*, Wiley, Hoboken, NJ 1998.
- [38] J. Sun, E. Timurdogan, A. Yaacobi, E. S. Hosseini, M. R. Watts, *Nature* **2013**, 493, 195.
- [39] Z. Yaqoob, D. Psaltis, M. S. Feld, C. Yang, *Nat. Photonics* **2008**, 2, 110.
- [40] D. G. Grier, *Nature* **2003**, 424, 810.
- [41] Y. Zhang, T. Chang, B. Zhou, Y. Cui, H. Yan, Z. Liu, F. Schmitt, J. Lee, R. Moore, Y. Chen, H. Lin, H. Jeng, S. Mo, Z. Hussain, A. Bansil, Z. Shen, *Nat. Nanotech.* **2014**, 9, 111.
- [42] C. Yan, J. Liu, Y. Zang, J. Wang, Z. Wang, P. Wang, Z. Zhang, L. Wang, X. Ma, S. Ji, K. He, L. Fu, W. Duan, Q. Xue, X. Chen, *Phys. Rev. Lett.* **2014**, 112, 186801.
- [43] J. Zeng, X. Wang, J. Sun, A. Pandey, A. N. Cartwright, N. M. Litchinitser, *Sci. Rep.* **2013**, 3, 2826.
- [44] H. J. Caulfield, S. Dolev, *Nat. Photonics* **2010**, 4, 261.
- [45] J. L. Schwartz, M. A. Peck, C. D. Hall, *J. Guid. Control Dyn.* **2003**, 26, 513.
- [46] P. Zhou, J. H. Burge, *Appl. Opt.* **2007**, 46, 657.
- [47] H. F. Ma, T. J. Cui, *Nat. Commun.* **2010**, 1, 21.
- [48] F. Samaeifar, H. Hajghassem, A. Afifi, H. Abdollahi, *Sensor Rev.* **2015**, 35, 116.
- [49] M. C. Çakir, D. Çalışkan, B. Bütün, E. Özbay, *Sensors* **2016**, 16, 1612.
- [50] Z. Yang, C. Ko, S. Ramanathan, *Annu. Rev. Mater. Res.* **2011**, 41, 337.
- [51] R. Kirchain, L. Kimerling, *Nat. Photonics* **2007**, 1, 303.